

# First Report of Chenodeoxycholic Acid–Substituted Dyes Improving the Dye Monolayer Quality in Dye-Sensitized Solar Cells

Audun F. Buene, David M. Almenningen, Anders Hagfeldt, Odd R. Gautun, and Bård H. Hoff\*

Chenodeoxycholic acid (CDCA) is the most used antiaggregation additive in dye-sensitized solar cells since its introduction to the field in 1993. However, effective suppression of dye aggregation comes at the cost of reduced dye loading, a lower open-circuit voltage, and limited control of dye/additive distribution when cosensitizing with free CDCA. To combat this, herein, a novel dye design concept that uses the covalent attachment of a CDCA moiety to triarylamine sensitizers is reported. The CDCA substituents do not affect the photophysical or electrochemical properties of the sensitizers but have a positive effect on the photovoltaic performance with  $[\text{Cu}^{+/2+}(\text{tmby})_2](\text{TFSI})_{1/2}$  electrolyte (tmby = 4,4',6,6'-tetramethyl-2,2'-bipyridine, TFSI = bis(trifluoromethanesulfonyl)imide). By ensuring a one-to-one ratio of dye and CDCA, paired with isotropic distributions of each component, this approach results in a higher-quality dye monolayer. Compared with the reference system, the novel approach reported herein gives a higher open-circuit voltage and power conversion efficiency (PCE). The best device is fabricated with the dye C<sub>6</sub>-CDCA, delivering a PCE of 6.84% ( $8 \mu\text{m TiO}_2$ , 1 mM CDCA,  $J_{\text{SC}} = 8.64 \text{ mA cm}^{-2}$ ,  $V_{\text{OC}} = 1007 \text{ mV}$ , and  $\text{FF} = 0.77$ ).

is remarkably efficient compared with other long-established technologies such as GaAs solar cells, particularly under low-light conditions.<sup>[3]</sup> Flexible, semitransparent, and aesthetically decorative devices can be manufactured from low-cost materials.<sup>[4]</sup> As the most important components within DSSCs, the dyes themselves are currently the subject of extensive development and optimization.<sup>[5,6]</sup> Improvements in device architecture or electrolyte composition often spark the development of new dyes, which are more compatible with the new components.<sup>[7,8]</sup> Improving the efficiency of DSSCs through dye development is largely focused on enhancing the overall absorption properties, and increasing the size of the conjugated system is a popular method of achieving this. There is a drawback to the extensive conjugation, namely undesirable  $\pi$ - $\pi$  interactions. Intermolecular aggregation between dye molecules will increase

charge recombination and can be detrimental to device performance.<sup>[9]</sup>

A common strategy for reducing aggregation for both metal-complex dyes and organic sensitizers is the use of alkyl or alkoxy chains, present in just about all of the highest-performing sensitizers.<sup>[8,10–15]</sup> One of the more exciting examples of a novel antiaggregation unit was the use of a glucose derivative attached by click chemistry to a dianchoring phenothiazine sensitizer, reported by Manfredi et al. and demonstrated for dye-sensitized photocatalytic hydrogen production.<sup>[16]</sup>


Another antiaggregation approach was presented as early as 1993, by Kay and Grätzel.<sup>[17]</sup> Bile acids are compounds based on a steroid scaffold with one to three hydroxyl groups, in addition to a flexible chain with a carboxylic acid. Consequently, they are amphiphilic and chiral compounds. In biology they are well known to facilitate fat absorption; they are signaling molecules, affecting both nuclear and membrane receptors,<sup>[18]</sup> and are useful in various applications due to their tendency to form micelles.<sup>[19]</sup> Originally, bile acids were intended as additives for staining solutions, suppressing the formation of dye aggregates. These additives, such as chenodeoxycholic acid (CDCA), were later also found to anchor on the  $\text{TiO}_2$  surface. By suppressing unfavorable dye–dye interactions, CDCA has become the most widely used additive in DSSCs.

## 1. Introduction

Dye-sensitized solar cells (DSSCs) is a photovoltaic technology based on sensitized mesoscopic nanoparticles of a wide-bandgap semiconductor such as  $\text{TiO}_2$ .<sup>[1,2]</sup> Coupled with a counter electrode and an electrolyte, the complete photoelectrochemical cell

Dr. A. F. Buene, D. M. Almenningen, Prof. O. R. Gautun, Prof. B. H. Hoff  
Department of Chemistry  
Norwegian University of Science and Technology  
Høgskoleringen 5, NO-7491 Trondheim, Norway  
E-mail: bard.h.hoff@ntnu.no

Prof. A. Hagfeldt  
Laboratory of Photomolecular Science  
Institute of Chemical Sciences and Engineering  
École Polytechnique Fédérale de Lausanne (EPFL)  
Chemin des Alambics, Station 6, CH-1015 Lausanne, Switzerland

 The ORCID identification number(s) for the author(s) of this article can be found under <https://doi.org/10.1002/solr.201900569>.

© 2020 The Authors. Published by WILEY-VCH Verlag GmbH & Co. KGaA, Weinheim. This is an open access article under the terms of the Creative Commons Attribution-NonCommercial License, which permits use, distribution and reproduction in any medium, provided the original work is properly cited and is not used for commercial purposes.

DOI: 10.1002/solr.201900569

For steric reasons, cosensitization with CDCA leads to a reduction in dye loading. Furthermore, the additional carboxylic acids in the staining solution increase the degree of protonation of  $\text{TiO}_2$ . The expected effect is a lowering of the conduction band edge of titania, which in most cases leads to a reduction in  $V_{\text{OC}}$ . Maximizing the positive effects of CDCA is a careful balancing act in most scenarios, and the only real measure available to the researcher is to vary the concentration of CDCA. It was early established that quite large CDCA concentrations were necessary to compete with dye molecules for adsorption onto the  $\text{TiO}_2$  surface.<sup>[17]</sup> The exact ratio of dye to additive will vary between dyes and solvent systems, but additive concentrations 10–100 times higher than those of the dye are frequently reported in the literature.<sup>[20–23]</sup> Screening a range of CDCA concentrations is a common strategy. Despite optimizing the amount of coadsorbent, the researcher still has little control over the distribution of dye and additive with the conventional approach, as shown in **Figure 1**.

Herein we report the first examples of sensitizers with chenodeoxycholic substituents. The dyes differ by the length of the alkoxy chains on the donor moiety ( $\text{C}_3\text{H}_7$  vs  $\text{C}_6\text{H}_{13}$ ), which

is likely to affect the antiaggregation properties of dyes. With this approach, we improve the distribution of CDCA moieties, achieving a higher-quality self-assembled monolayer (SAM). Simultaneously, this reduces the total number of carboxylate anchoring groups on  $\text{TiO}_2$ , increasing  $V_{\text{OC}}$ . Two control sensitizers without CDCA substituents, but otherwise identical, were also prepared for the effects of the CDCA substituents to be measured. The choice of triarylamine as dye scaffold enables the use of novel copper electrolytes in the DSSC devices. With copper electrolytes, the energy loss in dye regeneration is significantly reduced compared with conventional  $\text{I}^-/\text{I}_3^-$  electrolytes.<sup>[24,25]</sup> The thiophene–furan  $\pi$ -spacer has recently been successfully used in a number of DSSC studies.<sup>[26–30]</sup> More importantly, this  $\pi$ -spacer proved suitable as a point of attachment for the very large CDCA substituent without inducing excessive ring twisting and was therefore selected for this study. In addition, this point of attachment places the CDCA substituent in a position comparable with that of free CDCA when anchored on the  $\text{TiO}_2$  surface.

## 2. Results and Discussion

The aim for this work was to improve the SAM quality by the covalent attachment of CDCA to the dye structure. This design was chosen to improve the distribution of dyes and additives in the SAM and reduce the total number of molecules anchored on the  $\text{TiO}_2$  surface, with the intention of achieving an overall higher power conversion efficiency (PCE) and increased  $V_{\text{OC}}$ . Recently, triarylamine-based sensitizers have achieved outstanding results in DSSCs, using novel cobalt and copper electrolytes.<sup>[8,24,31–35]</sup> Hence, this popular dye class became the foundation of the study.

It was also essential that the large CDCA substituent did not induce any ring twisting of the conjugated system, which could negatively affect the optical properties of the sensitizers. To minimize any potential ring twisting, the CDCA substituent was attached in the bay region between two five-membered heterocycles.

### 2.1. Dye Synthesis

#### 2.1.1. Donor Moiety

The complexity of the target sensitizers meant the preparation resembled more of a total synthesis than the synthesis of a simple dye. The preparation of the donor fragments however was relatively uncomplicated, as shown in **Scheme 1**. Synthesis routes based on those reported by Gabriellson et al. and Zhang et al. were used to prepare the triarylamine donor fragments.<sup>[10,36]</sup> While (2,4-dipropoxyphenyl)boronic acid was commercially available, 2-(2,4-bis(hexyloxy)phenyl)-pinacol boronic ester had to be prepared in-house, using the convenient palladium-catalyzed borylation reaction developed by Billingsley and Buchwald.<sup>[37]</sup> The crude pinacol boronic ester was used without further purification to yield triarylamine 3. The last bromination step by *N*-bromosuccinimide (NBS) proved regioselective with high yields of the advanced intermediates 4 and 5.

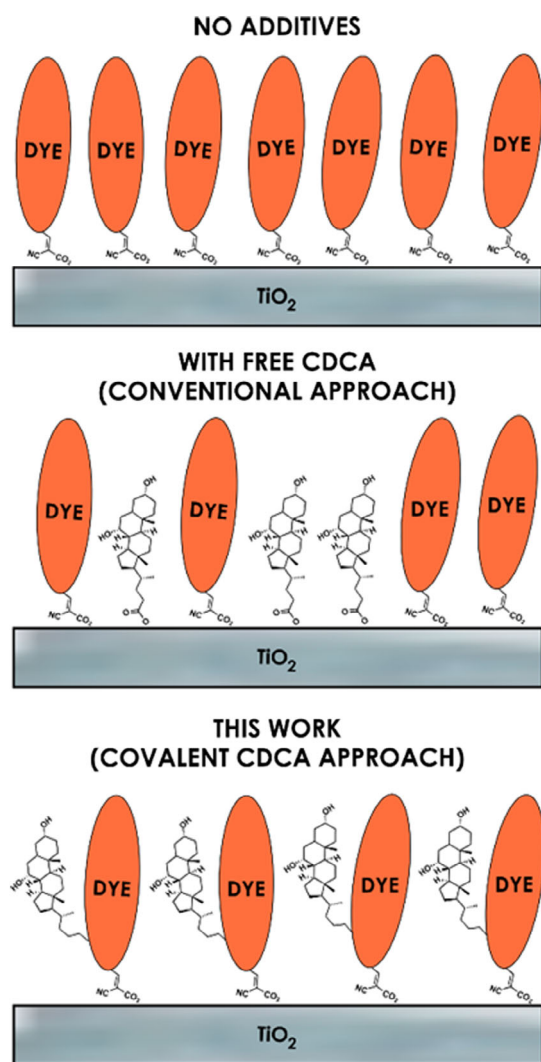
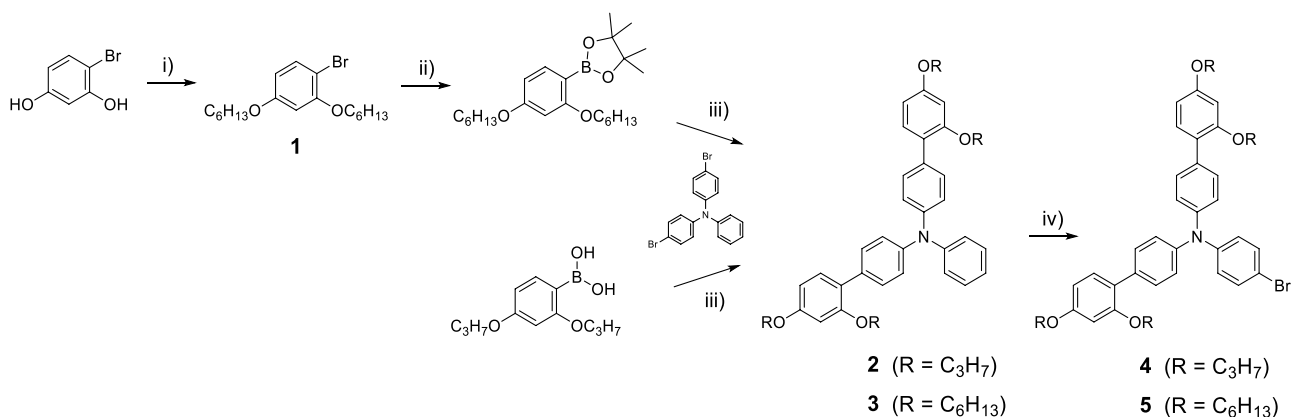


**Figure 1.** Dye and additive distribution concepts.



**Scheme 1.** Synthesis route of triphenylamine donor fragments. i) KOH, DMSO, 1-bromohexane, r.t., ii) HBpin, PdCl<sub>2</sub>(CH<sub>3</sub>CN)<sub>2</sub>, SPhos, Et<sub>3</sub>N/1,4-dioxane, 110 °C, iii) Pd(OAc)<sub>2</sub>, SPhos, K<sub>2</sub>CO<sub>3</sub>, H<sub>2</sub>O/1,4-dioxane, iv) NBS, CH<sub>2</sub>Cl<sub>2</sub>, r.t.

### 2.1.2. $\pi$ -Spacer Moiety

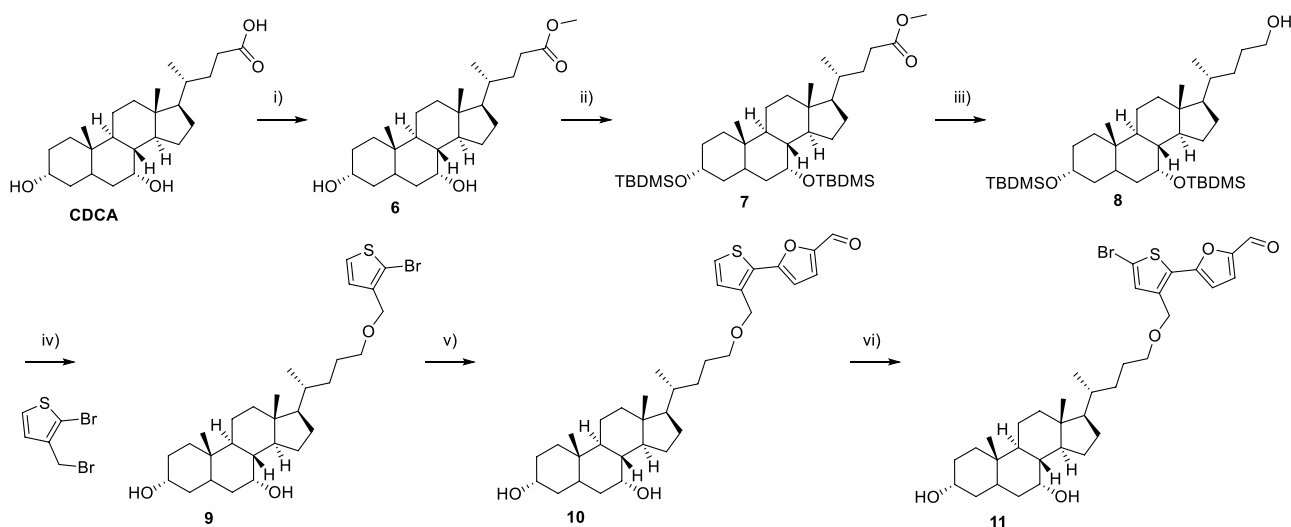
Our strategy to arrive at the CDCA-functionalized  $\pi$ -spacer involved several different reactions, from old textbook chemistry to more modern coupling reactions (see **Scheme 2**). First, CDCA was converted to its methyl ester **6**, in a Fischer esterification. Second, the hydroxyl groups of **6** were protected as *tert*-butyldimethylsilyl ethers (TBDMS), and compound **7** was further reduced by LiAlH<sub>4</sub> in tetrahydrofuran (THF) to yield the primary alcohol **8**. To install the CDCA moiety onto the  $\pi$ -spacer, a Williamson ether synthesis between compound **8** and 2-bromo-3-(bromomethyl)thiophene based on the procedure reported by Bjørnholm et al. was performed.<sup>[38]</sup> Subsequently, the removal of the TBDMS protected groups by HCl gave compound **9**. The first four steps were all quantitative in terms of yields (97–99%). The introduction of the furan moiety proved to be a challenging step, but a Suzuki coupling catalyzed by [1,1'-bis(diphenylphosphino)ferrocene]dichloropalladium(II) (PdCl<sub>2</sub>(dppf)) using three equivalents of (5-formylfuran-2-yl)boronic acid was eventually

developed, giving compound **10** in a satisfactory yield of 68%. The final step in the synthesis of the CDCA  $\pi$ -spacer building block **11** was bromination by NBS. Despite the low yield of 25% due to a challenging purification, enough material was prepared for the target sensitizers to be synthesized in sufficient amounts.

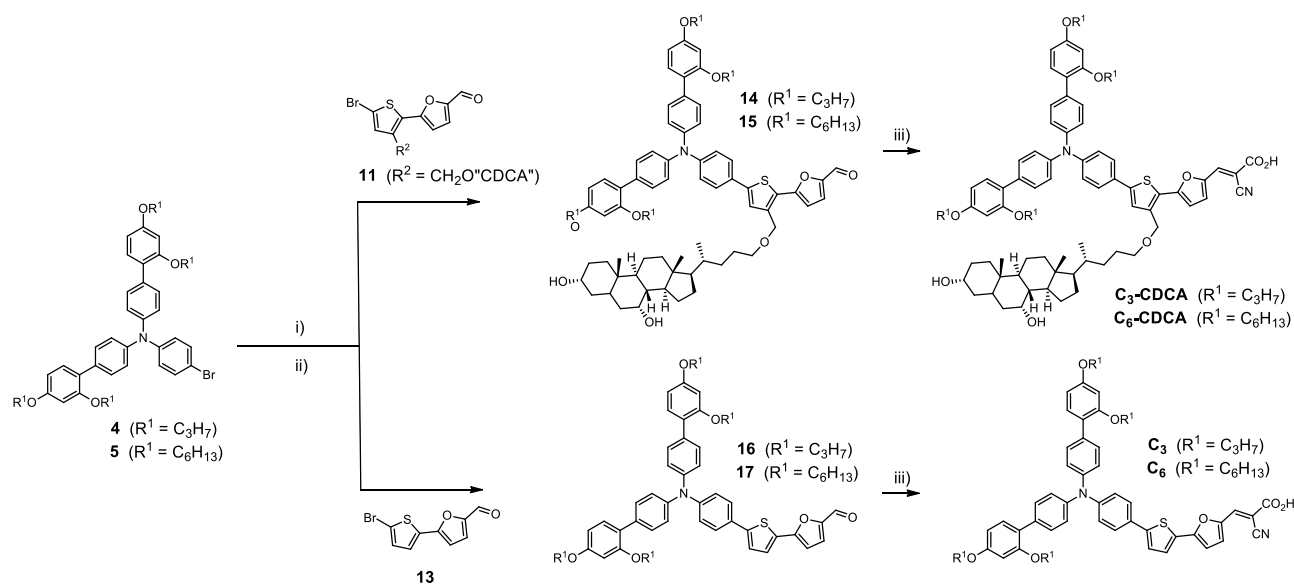
Preparation of the  $\pi$ -spacer without the CDCA substituent required two steps. First, a Suzuki coupling between 2-bromothiophene and 5-formylfuran-2-yl boronic acid gave compound **12** in 48% yield, confirming it was not the steric bulk of the CDCA substituent that caused the low yield in the same reaction to compound **10**. Finally, a bromination by NBS in 59% yield completed the reference  $\pi$ -spacer building block **13**.

### 2.1.3. Dye Assembly

The triarylamine donor fragments **4** and **5** were converted to boronic esters again by the procedure of Billingsley and Buchwald.<sup>[37]</sup> They were then coupled to the  $\pi$ -spacer building



**Scheme 2.** Synthesis route for CDCA-functionalized  $\pi$ -spacer **11**. i) MeOH, H<sub>2</sub>SO<sub>4</sub>, r.t., ii) TBDMS triflate, 2,6-lutidine, DCM, r.t., iii) LiAlH<sub>4</sub>, THF, r.t., iv) NaH, THF, 60 °C followed by deprotection by HCl, v) (5-formylfuran-2-yl)boronic acid, PdCl<sub>2</sub>(dppf), K<sub>2</sub>CO<sub>3</sub>, H<sub>2</sub>O/1,4-dioxane, 80 °C, vi) NBS, CHCl<sub>3</sub>/AcOH, 0 °C.



**Scheme 3.** Fusion of triphenylamine donors **4** and **5** with the CDCA-functionalized  $\pi$ -spacer **11** and reference  $\pi$ -spacer **13**. i) HBpin,  $\text{PdCl}_2(\text{CH}_3\text{CN})_2$ , SPhos,  $\text{Et}_3\text{N}/1,4\text{-dioxane}$ ,  $110^\circ\text{C}$ , ii)  $\text{Pd}(\text{OAc})_2$ , SPhos,  $1,4\text{-dioxane}/\text{H}_2\text{O}$ ,  $80^\circ\text{C}$ , iii) cyanoacetic acid, piperidine, ACN/THF,  $65^\circ\text{C}$ .

blocks **11** and **13**, giving the carboxaldehydes **14**–**17**, as shown in **Scheme 3**. The Knoevenagel condensation installed the cyanoacrylic acid anchoring group in yields from 54% to 95%, successfully concluding the synthesis of the first two sensitizers bearing CDCA substituents and their two corresponding reference dyes.

## 2.2. Photophysical Properties

One aim with the design of the sensitizers is that the CDCA substituent does not negatively affect their photophysical and electrochemical properties. The CDCA moiety should simply be an inert substituent, affecting only the aggregation properties of the dyes. The UV–vis spectra shown in **Figure 2** show only minor differences in absorption between the four sensitizers. The reference dyes **C<sub>3</sub>** and **C<sub>6</sub>** have slightly higher molar extinction coefficients, and the internal charge transfer (ICT) transition

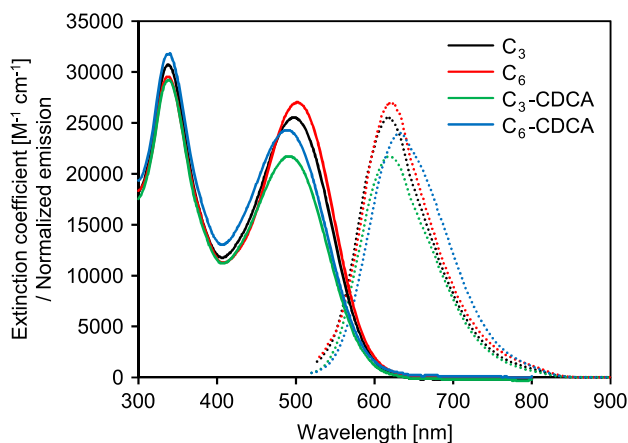


**Figure 2.** UV–vis measurements and normalized emission spectra of all dyes in dichloromethane solution.

peaks are redshifted by about 10 nm. These changes can simply be explained by the large CDCA substituent introducing a slight ring twist between the thiophene and furan rings. Of the four dyes, the two with **C<sub>6</sub>** chains have 6–12% higher molar extinction coefficients compared with the **C<sub>3</sub>** analogs. Although the reason for this is unknown, the phenomenon of higher molar extinction coefficients for longer alkyl chains has been previously observed for triarylamine,<sup>[39]</sup> phenothiazine,<sup>[40]</sup> and ruthenium complex dyes.<sup>[41]</sup>

When anchored on  $\text{TiO}_2$  without additional coadsorbents (Figure S1, Supporting Information), the ICT transition peaks of the reference sensitizers are blueshifted by 53–59 nm, indicating they could be prone to H aggregation.<sup>[9]</sup> Sensitizers **C<sub>3</sub>-CDCA** and **C<sub>6</sub>-CDCA** are also affected but by a reduced margin of 35–44 nm. This suggests that the CDCA substituents prevent aggregation to a certain extent and that additional CDCA added to the staining solution may be required when fabricating devices. The free OH groups of the tethered CDCA substituent may well interact with the semiconductor surface, due to the flexibility of the linker, but the extent and effect of this has not been investigated.

Optical bandgaps extracted from the intersections of the absorption and emission curves in Figure 2 are in the range of 2.18–2.20 eV for all four sensitizers, further indicating that CDCA substituents do not significantly affect the photophysical properties. Integration of the 1 sun AM1.5 G solar spectrum gives the maximum short-circuit current obtainable from a sensitizer with a specific absorption onset or bandgap. For the sensitizers in this work, with a bandgap around 2.20 eV, a maximum  $J_{\text{SC}}$  value of  $10.4 \text{ mA cm}^{-2}$  is expected. All the measured photophysical and electrochemical properties are shown in **Table 1**.

## 2.3. Electrochemical Properties

The four dyes adsorbed onto  $\text{TiO}_2$  films were investigated by cyclic voltammetry (CV) to determine the oxidation potentials.

**Table 1.** Photophysical properties of the triarylamine dyes  $C_3$ ,  $C_6$ ,  $C_3$ -CDCA, and  $C_6$ -CDCA.

Dye	$\lambda_{\text{abs}}^{\text{a)}$ [nm]	$\epsilon$ [ $M^{-1} \text{ cm}^{-1}$ ]	Em. <sup>b)</sup> [nm]	$\lambda_{\text{abs}}^{\text{c)}$ on $\text{TiO}_2$ [nm]	Rel. $\epsilon$ on $\text{TiO}_2$	$E_{0-0}^{\text{d)}$ [eV]	$E_{\text{ox}}^{\text{e)}$ [V vs SHE]	$E_{\text{LUMO}}^{\text{f)}$ [V]
$C_3$	498	25 500	617	442	1.43	2.20	1.09	-1.11
$C_6$	502	27 000	621	445	1.29	2.19	1.12	-1.07
$C_3$ -CDCA	492	21 700	619	448	1.00	2.20	1.11	-1.09
$C_6$ -CDCA	489	24 300	632	451	1.01	2.18	1.11	-1.07

<sup>a)</sup>Maximum of most redshifted peak; <sup>b)</sup>Emission when ICT band is excited, in DCM solution; <sup>c)</sup>Maximum of most redshifted peak on  $\text{TiO}_2$  (2.5  $\mu\text{m}$ , GreatcellSolar 18NR-T); <sup>d)</sup>Calculated from the intersection of the absorption and normalized emission spectra; <sup>e)</sup>Measured versus  $F_c^+/F_c$  on stained  $\text{TiO}_2$  electrodes in acetonitrile with 0.1 M LiTFSI, converted to V versus SHE by 0.624. Scan rate 20  $\text{mV s}^{-1}$ ; <sup>f)</sup>Calculated from  $E_{\text{ox}} - E_{0-0}$ .

The 2.5  $\mu\text{m}$  thick films were prepared by 30NR-D  $\text{TiO}_2$  screen printed on FTO glass. The stained photoanodes were attached to the working electrode of the potentiostat, with a carbon graphite rod used as a counter electrode. The reference electrode was Ag/AgCl and the supporting electrolyte was 0.1 M lithium bis(trifluoromethanesulfonyl)imide (LiTFSI) in dry acetonitrile. Cyclic voltammograms are shown in **Figure 3**, and the extracted electrochemical information is found in Table 1. All the dyes display a single reversible oxidation and very similar electrochemical behavior. This indicates that neither the presence of the CDCA substituent nor the length of the alkoxy chains greatly

affects the electrochemical properties of the sensitizers. When the ferrocene standard was measured, the working electrode was replaced by a glassy carbon electrode, and the  $E_{1/2}$  of ferrocene was found at 0.36 V versus Ag/AgCl. The calculated values for the oxidation potentials of the four sensitizers were all in the range of 1.09–1.12 V versus standard hydrogen electrode (SHE), suggesting that they should be compatible with the redox potential of the  $[\text{Cu}^{+/2+}(\text{tmby})_2](\text{TFSI})_{1/2}$  electrolyte ( $\text{tmby} = 4,4',6,6'$ -tetramethyl-2,2'-bipyridine), reported at 0.87 V versus SHE.<sup>[24]</sup> Excited state energies calculated from the  $E_{0-0}$  values and  $E_{\text{ox}}$  were found between -1.07 and -1.11 V versus SHE, suggesting that all sensitizers provide a sufficient driving force for efficient electron injection into the conduction band of  $\text{TiO}_2$ , commonly reported around -0.5 V versus SHE. The energy levels would also be compatible with the  $\text{I}^-/\text{I}_3^-$  electrolyte, but this would lower the  $V_{\text{OC}}$  significantly, and we are of the opinion that the same relative effects on performance would be observed.

#### 2.4. Photovoltaic Properties

The four sensitizers were evaluated in DSSCs alongside the structurally related reference dye D35 reported by Hagberg et al.<sup>[43]</sup> The fabrication procedure for the DSSCs is described in the Experimental Section. The complete set of photovoltaic data is reported in Table 2, while a selection of  $J$ - $V$  curves is shown in **Figure 4a,b**.

First, the effect of CDCA as a coadsorbent for the reference sensitizers  $C_3$  and  $C_6$  was determined by testing a range of CDCA concentrations (0, 1, 5, 10, and 50 equivalents relative to the sensitizers). The results of this study are shown in **Figure 5** and in the top part of Table 2. The full set of  $J$ - $V$  curves and the incident photon-to-current conversion efficiency (IPCE) spectra of all CDCA concentrations are included in the Supporting Information (Figure S2, Supporting Information).

Generally,  $C_6$  outperforms  $C_3$  in all performance characteristics in the CDCA concentration study, despite having a 19% reduction in dye loading compared with  $C_3$  (Table S1, Supporting Information). Further, the performance of  $C_3$  is also affected to a greater extent by the CDCA concentration than that of  $C_6$ . The most noticeable difference between the two dyes, differing only by the alkoxy chain length, is the open-circuit voltage. Without the CDCA additive, the difference in  $V_{\text{OC}}$  is 99 mV in favor of dye  $C_6$ . When including the D35 reference dye, which has butoxy

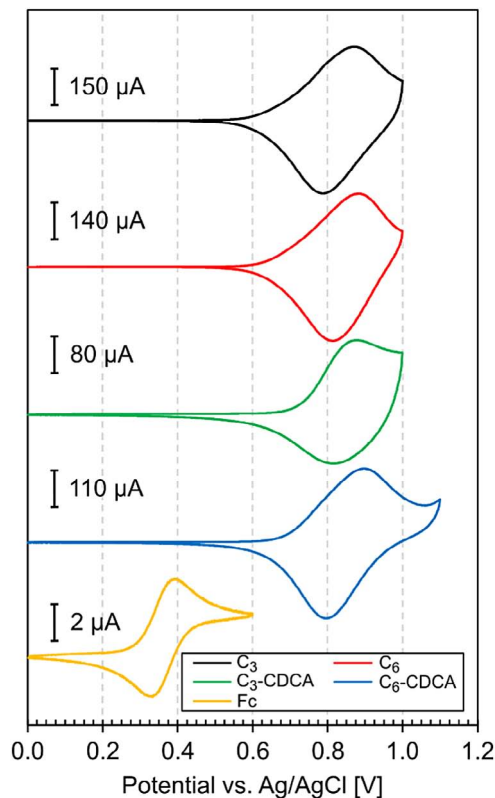


**Figure 3.** CVs of the four sensitizers and ferrocene. Sensitizers measured on  $\text{TiO}_2$  films (2.5  $\mu\text{m}$  on FTO glass), carbon counter electrode, Ag/AgCl reference, 0.1 M LiTFSI supporting electrolyte. Ferrocene (Fc) was measured with a glassy carbon working electrode and used for calibration with a value of 0.624 V versus SHE.<sup>[42]</sup>



**Table 2.** Photovoltaic performance of all dyes in 1 sun AM 1.5 G illumination and from IPCE measurements. Electrolyte composition 0.09 M [Cu(tmby)<sub>2</sub>] TFSI<sub>2</sub>, 0.20 M [Cu(tmby)<sub>2</sub>]TFSI, 0.1 M LiTFSI, and 0.6 M 1-methylbenzimidazole in dry acetonitrile.

Dye	CDCA [eq.]	TiO <sub>2</sub> [μm]	IPCE $J_{sc}$ [mA cm <sup>-2</sup> ] <sup>a)</sup>	$J_{sc}$ [mA cm <sup>-2</sup> ]	$V_{oc}$ [mV]	Fill factor [%]	PCE [%]
C <sub>3</sub>	0	4 + 2	6.31	6.53 ± 0.13	965 ± 3	0.72 ± 0.01	4.55 ± 0.12
	1	4 + 2	6.91	6.88 ± 0.43	965 ± 10	0.73 ± 0.01	4.91 ± 0.42
	5	4 + 2	7.04	7.29 ± 0.27	955 ± 14	0.72 ± 0.01	5.05 ± 0.28
	10	4 + 2	6.88	7.60 ± 0.14	962 ± 20	0.73 ± 0.02	5.37 ± 0.23
	50	4 + 2	6.32	6.88 ± 0.40	937 ± 8	0.72 ± 0.04	4.69 ± 0.50
C <sub>6</sub>	0	4 + 2	7.68	7.09 ± 0.14	1064 ± 5	0.72 ± 0.01	5.48 ± 0.14
	1	4 + 2	7.96	7.27 ± 0.32	1038 ± 28	0.74 ± 0.02	5.64 ± 0.26
	5	4 + 2	6.96	7.56 ± 0.08	970 ± 21	0.73 ± 0.02	5.39 ± 0.20
	10	4 + 2	7.26	7.56 ± 0.18	1000 ± 22	0.74 ± 0.01	5.65 ± 0.14
	50	4 + 2	6.18	7.19 ± 0.09	959 ± 13	0.76 ± 0.01	5.29 ± 0.15
C <sub>3</sub> -CDCA	0	4 + 2	6.49	5.55 ± 0.09	1025 ± 5	0.70 ± 0.01	4.03 ± 0.04
	0	8 + 4	6.98	6.21 ± 0.43	961 ± 11	0.74 ± 0.02	4.49 ± 0.46
	10	4 + 2	7.27	7.12 ± 0.17	1013 ± 15	0.73 ± 0.01	5.34 ± 0.24
	10	8 + 4	8.05	7.50 ± 0.39	1000 ± 2	0.76 ± 0.01	5.81 ± 0.32
C <sub>6</sub> -CDCA	0	4 + 2	6.77	7.07 ± 0.08	1044 ± 3	0.72 ± 0.02	5.39 ± 0.07
	0	8 + 4	8.54	7.84 ± 0.47	1008 ± 25	0.76 ± 0.01	6.11 ± 0.44
	10	4 + 2	7.81	8.00 ± 0.09	1035 ± 15	0.74 ± 0.00	6.20 ± 0.02
	10	8 + 4	8.54	8.30 ± 0.30	992 ± 14	0.77 ± 0.02	6.44 ± 0.35
D35	0	4 + 2	7.40	7.51 ± 0.22	1016 ± 23	0.73 ± 0.00	5.60 ± 0.31

<sup>a)</sup>Obtained by integration of the IPCE spectrum over the 1 sun AM 1.5 G spectrum.

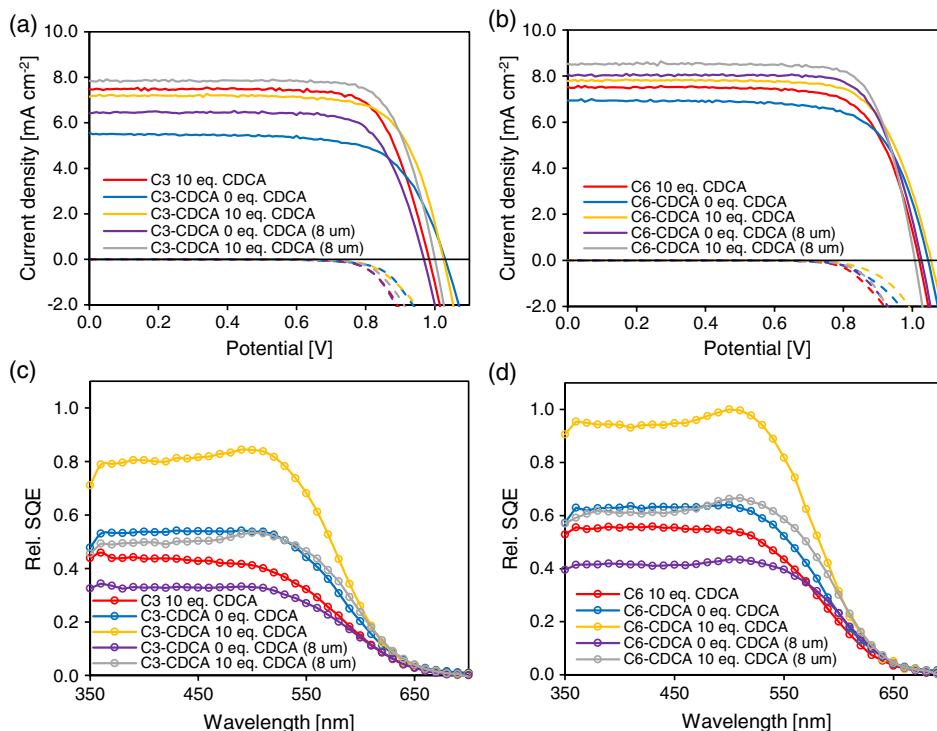


**Figure 4.** a,b) Current density versus applied potential plots under 1 sun AM1.5 G illumination (lines) and in the dark (dashed lines). c,d) SQE spectra, essentially dye-loading-adjusted incident photon-to-current conversion efficiency curves. Curves are scaled relative to the highest-performing device. Comment of 8 μm means 8 + 4 μm TiO<sub>2</sub> was used, whereas no specification implies 4 + 2 μm TiO<sub>2</sub> electrodes. Original IPCE measurements available in the Supporting Information.

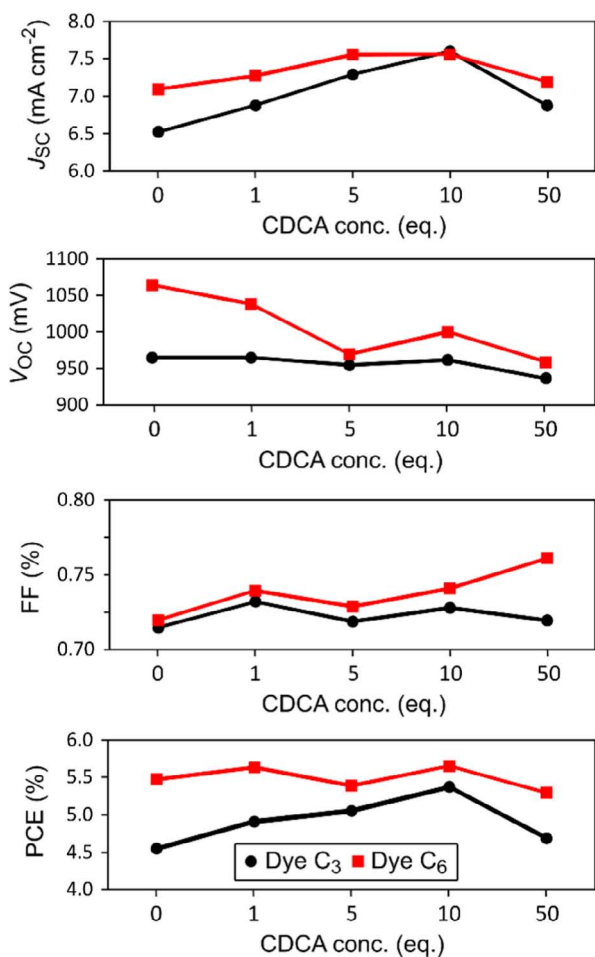


**Figure 5.** Screening of CDCA concentration for dyes C<sub>3</sub> and C<sub>6</sub>. Each data point is the average of three devices.

chains, the following trend of  $V_{OC}$  is found: C<sub>3</sub> (965 mV) < C<sub>4</sub> (1016 mV) < C<sub>6</sub> (1064 mV). As the CDCA concentration is increased, the  $V_{OC}$  of both dyes decreases. This is explained by a lowered conduction band edge due to protonation of TiO<sub>2</sub> by the carboxylic acid of CDCA. The maximum short-circuit current density is found for 5–10 equivalents of CDCA, leading to the highest PCEs being obtained for 10 equivalents of CDCA for both chain lengths.

With the coadsorbent dependence of the reference sensitizers determined, the dyes with CDCA substituents were tested with no additional CDCA additive. Compared with the optimized C<sub>3</sub> and C<sub>6</sub> devices, the relative efficiencies were 75% and 95% for C<sub>3</sub>-CDCA and C<sub>6</sub>-CDCA. This is particularly notable when considering that the CDCA substituent reduces the dye loading by 39–45%. Perhaps most strikingly, the increase in  $V_{OC}$  from C<sub>3</sub> to C<sub>3</sub>-CDCA was measured at 60 mV. In other studies, the use of longer alkoxy chains has produced the same  $V_{OC}$ -enhancing behavior,<sup>[44]</sup> and thus we conclude that the CDCA substituent blocks electron recombination from TiO<sub>2</sub> to the electrolyte and thereby improves the photovoltage. This is supported by a slight improvement in electron lifetimes (see Figure 6c). A similar behavior has previously been reported for the introduction of

an alkyl chain in the same position of a dye with a comparable structure. The LEG3 dye, with the hexyl entity attached to the  $\pi$ -spacer, displayed increased  $J_{SC}$ ,  $V_{OC}$ , and fill factor, attributed to the reduced recombination when compared with the reference dye LEG1.<sup>[36]</sup> Following the same arguments, for the C<sub>6</sub> dyes, no change in  $V_{OC}$  was observed, or expected, as the longer alkoxy chains already sufficiently block the recombination.

We then tested the optimized CDCA coadsorbent concentrations (10 equivalents) with the dyes C<sub>3</sub>-CDCA and C<sub>6</sub>-CDCA. To our surprise, this further improved the efficiencies significantly. In the case of C<sub>3</sub>-CDCA with 10 equivalent CDCA, a near-identical PCE as for the optimized C<sub>3</sub> was achieved, an improvement of 33%. For C<sub>6</sub>-CDCA, the additional coadsorbent gave an improvement in PCE of 10%. Obviously, more than one unit of CDCA per dye molecule is required for the sensitizer to operate efficiently. Furthermore, because C<sub>6</sub>-CDCA is more efficient than C<sub>6</sub> with the same amount of CDCA in the staining solution, it could indicate an improved distribution of CDCA, so a higher short-circuit current can be obtained despite lowered dye-loading values (see Table S1, Supporting Information).

Finally, for dyes C<sub>3</sub>-CDCA and C<sub>6</sub>-CDCA, we attempted to double the thickness of the TiO<sub>2</sub> layers, from 4 + 2 to 8 + 4  $\mu\text{m}$  (see Table 2). This resulted in an increased average PCE of 9%, suggesting that the optimal thickness of active TiO<sub>2</sub> in this study is between 4 and 8  $\mu\text{m}$ . The observed reduction in the open-circuit voltage can be explained by a more restricted diffusion for the redox shuttle in the TiO<sub>2</sub> network, increasing recombination and thus lowering the electron lifetime and  $V_{OC}$ . Surprisingly, the fill factors of the devices increased with thicker TiO<sub>2</sub> films, which is not expected under full illumination if there are diffusion issues in the devices.

The IPCE spectra in Figure S3, Supporting Information, show that light harvest is less than optimal for all devices fabricated with these sensitizers, as the maximum IPCE value is only 70%. This is a consequence of modest molar extinction coefficients, paired with thin TiO<sub>2</sub> layers required for the slow diffusing copper complex redox couple in the electrolyte. However, for the purpose of testing the CDCA substituents, this is of little importance. The IPCE spectra resemble the UV-vis absorption spectra, but the onset is redshifted by up to 50 nm, compared with the absorption spectra, likely an effect of different solvents in device operation and the photophysical measurements. From Table 2, the values for the integrated short-circuit current from the IPCE spectra are in good agreement with the values obtained from the  $J$ - $V$  sweeps.

It was desirable to develop a technique capable of distinguishing between devices fabricated with varying quality SAMs but with similar performance characteristics. This should also be of wider interest to the DSSC community, as there are currently few techniques for assessing the SAM quality. Our solution to this issue was to adjust the IPCE spectra for the respective dye-loading values, the results of which are shown in Figure 4c,d. This way, the photovoltaic contribution per sensitizer molecule can be displayed and compared, with the plot resembling an absorbed photon-to-current conversion efficiency (APCE) spectrum, as  $IPCE = APCE \cdot LHE$ , where LHE is the light-harvesting efficiency defined by International Union of Pure and Applied Chemistry (IUPAC) as  $1 - 10^{-A}$ , (where  $A$  is absorbance), which again is a product of the extinction

coefficient and dye loading of the sensitizer on the TiO<sub>2</sub> surface. However, for most thicker films, the LHE is close to 1 regardless of the sensitizer, making dye-loading values the more sensible choice for scaling the IPCE spectra. In addition, when comparing dyes of similar extinction coefficients, any differences in absorbance occur from the respective dye-loading values. To the best of our knowledge, this approach has not been used to investigate the individual efficiency contributions of sensitizers, and thus we suggest the term “sensitizer quantum efficiency” (SQE) for the technique. Although the use of absolute units like milliamperes per centimeter square per mol dye is possible for SQE, we here chose relative SQE to compare the different sensitizers.

High SQE values in these plots indicate high efficiencies of the individual sensitizer molecules, and low values can be an indication of recombination, diffusion issues, or poor absorption properties. Here, the performance advantage of the CDCA-substituted dyes is very clear for both the C<sub>3</sub> and C<sub>6</sub> dyes. First, with the same concentration of CDCA in the staining solutions, the C<sub>3</sub>/C<sub>6</sub>-CDCA dyes are remarkably more efficient than their unsubstituted analogs. This suggests a more optimized molecular environment for the CDCA dyes in the SAM. Second, by increasing the thickness of TiO<sub>2</sub>, the individual sensitizer performance is lowered. The mechanism behind this behavior must be related to either the increased redox shuttle diffusion resistance, electron transport resistance, or complete light attenuation, leaving a portion of the active layer without any illumination.

Charge extraction and electron lifetime measurements were used to further investigate the properties of the dye monolayers in the devices. In the charge extraction measurements of the C<sub>3</sub> dyes, the same V<sub>OC</sub> trend observed from the J–V sweeps can be

seen. The CDCA substituent shifts the curves toward higher V<sub>OC</sub> values, as well as toward higher Q<sub>OC</sub> values. For the C<sub>6</sub> dyes (Figure 6b), the trend is not as clear; this would be expected from the very similar photovoltaic performance. However, the devices with an 8 μm thick active TiO<sub>2</sub> layer deliver slightly higher Q<sub>OC</sub> values compared to the 4 μm devices.

The effect of different CDCA concentrations (0, 10, and 50 equivalents) has the same effect on the electron lifetime behavior for both C<sub>3</sub> and C<sub>6</sub>. An increased amount of CDCA causes a drop in electron lifetime, even though the relative conduction band shift associated with the protonation from the carboxylic acid of CDCA is accounted for. The same separated grouping of C<sub>3</sub> and C<sub>3</sub>-CDCA dyes is observed, suggesting the CDCA substituent is contributing to an overall denser dye/CDCA monolayer, restricting the access to TiO<sub>2</sub> for the Cu<sup>2+</sup> species. However, C<sub>6</sub> and C<sub>6</sub>-CDCA do not display the same trend. The reason for this could be superior antiaggregation properties of the hexyl chains over the propyl chains or a more efficient blocking effect of TiO<sub>2</sub>. Somewhat surprisingly, the thicker TiO<sub>2</sub> electrodes display the highest electron lifetimes in both C<sub>3</sub> and C<sub>6</sub> dye series. We expected the hindered diffusion of the copper redox species in and out of the TiO<sub>2</sub> layer to facilitate recombination of injected electrons to the electrolyte, but it appears that the quality of the monolayer is sufficiently high to block this recombination pathway.

To investigate the linearity of the devices, the photovoltaic performance of the highest-performing solar cells was measured under a range of light intensities (see Figure 7). A nonlinear short-circuit current density (as a function of light intensity) would indicate diffusion limitations. We suspected that the

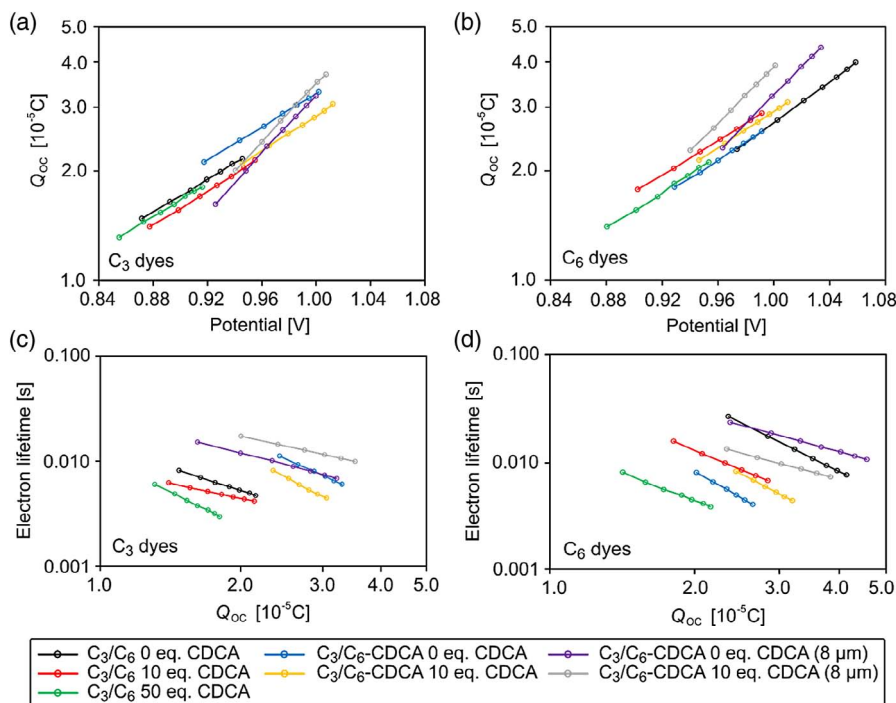


**Figure 6.** a,b) Charge extraction measurements at different light intensities. C<sub>3</sub> dyes in (a) and C<sub>6</sub> dyes in (b). c,d) Lifetime measurements at different light intensities, plotted against collected charge for the same devices at the same potentials. C<sub>3</sub> dyes in (c) and C<sub>6</sub> dyes in (d). Measured with the Dynamo Toolbox instrument.



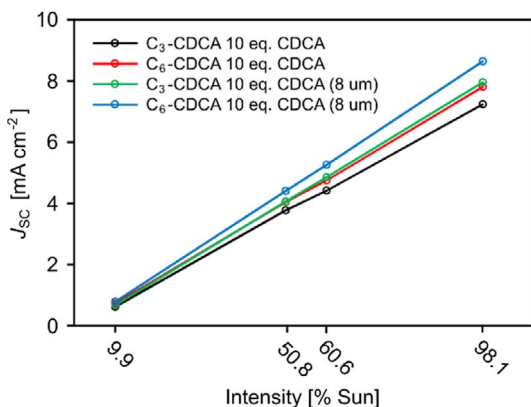


**Figure 7.** Short-circuit current measurements for four devices at light intensities from 0.1 to 1 sun. Comment of 8  $\mu\text{m}$  means 8 + 4  $\mu\text{m}$  TiO<sub>2</sub> was used, whereas no specification implies 4 + 2  $\mu\text{m}$  TiO<sub>2</sub> electrodes.

thicker devices with an 8  $\mu\text{m}$  active TiO<sub>2</sub> layer would be limited by diffusion issues, but all the devices behaved linearly from 0.1 to 1 sun AM1.5 G illumination. This indicates that diffusion does not limit the performance of the 8 + 4  $\mu\text{m}$  devices. It should be noted that the thicker scattering layer of the 8  $\mu\text{m}$  devices can play a role in enhancing the short-circuit current density and fully or partially mask any diffusion issues.

It is also possible that complete light attenuation in the thicker devices could be a limiting factor. This can explain the marginal performance enhancement, but not the lack of diffusion issues. To circumvent this, a sensitizer with a wider absorption spectrum or several dyes with complementary spectra will have to be used to increase the overall efficiency.

### 3. Conclusions

To solve the challenges often faced when using CDCA as an anti-aggregation additive in DSSCs, we reported a novel sensitizer design concept. By covalently attaching the CDCA moiety to the sensitizer, improved control of the dye monolayer composition was achieved. Two triarylamine dyes, carrying CDCA substituents, were prepared through a convergent 10–12-step synthesis. A thiophene–furan-linked  $\pi$ -spacer was found to be a convenient point of attachment of the CDCA moiety. Fortunately, the large bulk of the CDCA substituent did not affect the optical and electrochemical properties of the sensitizers, compared with the non-CDCA reference dyes.

First, it was established that the length of the alkoxy chains was of extreme importance in the devices fabricated with [Cu<sup>+2+</sup>(tmby)<sub>2</sub>](TFSI)<sub>1/2</sub> electrolyte. The  $V_{\text{OC}}$  of the C<sub>3</sub> dye was significantly lower than that of the C<sub>6</sub> dye. Although the  $V_{\text{OC}}$  of both dyes decreased upon addition of CDCA, 10 equivalents was found to yield the highest PCE values for the reference dyes. The covalent CDCA substituent of C<sub>6</sub>-CDCA was found to increase the  $V_{\text{OC}}$  compared with the optimized reference dye, and despite significantly lowering the dye loading, the PCE increased by 10%. This result is attributed to a higher-quality dye monolayer, as can be rationalized by SQE plots, a dye-loading-corrected IPCE measurement.

The dye molecules reported here are predominantly considered model compounds solely for testing the concept; however, larger effects are to be expected if this approach is implemented for severely aggregating dyes. Furthermore, the authors are of the opinion that the structure of CDCA should also be subject to optimization. Through synthetic efforts, the excellent anti-aggregation properties of CDCA may well be retained in a more compact unit.

### 4. Experimental Section

**Dye Synthesis:** The synthetic details for compounds **9**, **10**, **11**, **14**, and **15** and sensitizers C<sub>3</sub>-CDCA and C<sub>6</sub>-CDCA are included below. The synthetic procedures and spectroscopic data for the remaining compounds can be found in the Supporting Information. The reference list includes citations to works referenced in the Supporting Information.<sup>[45–50]</sup>

**Materials:** All chemicals and reagents used for the synthesis and device fabrication of the sensitizers were sourced from Sigma Aldrich. TiO<sub>2</sub> pastes were bought from GreatCell Solar and the D35 reference dye, [Cu(tmby)<sub>2</sub>](TFSI), and [Cu(tmby)<sub>2</sub>](TFSI)<sub>2</sub> were bought from Dyanamo.

**Solar Cell Assembly:** The working electrodes of the devices were fabricated from FTO glass (NSG10, Nippon Sheet Glass), cut to size, and washed with Deconex 21 (2 g L<sup>-1</sup>) in an ultrasonic bath for 45 min. Following UV/O<sub>3</sub> cleaning for 15 min (Novascan PSD-UV), a dense blocking layer of TiO<sub>2</sub> was deposited by immersion in aqueous TiCl<sub>4</sub> solution (40 mM) for 30 min at 70 °C. The glass slides were rinsed with deionized water and ethanol before the procedure was repeated and before heating the glass slides on a hotplate at 250 °C for 1 h. The titania pastes were screen printed onto the FTO glass with a 120 T mesh (Seritec Services S.A.), giving each electrode an active area of 0.283 cm<sup>2</sup>. For the 4 + 2  $\mu\text{m}$  electrodes, two layers of 30NR-D and one layer of scattering paste were printed, and for the electrodes with 8 + 4  $\mu\text{m}$ , four layers of 30NR-D and two layers of scattering paste were printed. Between each layer, the FTO glass slides were heated at 125 °C for 5 min and then cooled back to room temperature before printing the next layer. The working electrodes were finished by sintering on a programmable hotplate at 125, 250, 375, 450, and 500 °C for 5, 5, 5, 15, and 30 min with 5 min ramping between each step.

Counter electrodes were made from TEC15 FTO glass. Holes were drilled with a diamond drill bit, and the glass slides were washed in an ultrasonic bath for 15 min in each of the following solutions: Hellmanex 2% detergent solution, deionized water, ethanol, and acetone. A layer of poly(3,4-ethylenedioxythiophene) (PEDOT) was electrochemically deposited on the FTO glass from an aqueous solution of 3,4-ethylenedioxythiophene (EDOT), as described by Ellis et al.<sup>[51]</sup>

The solvent mixture used for the dye-staining solutions was acetonitrile/*tert*-butanol/tetrahydrofuran (1:1:1, v/v), with a dye concentration of 0.1 mM and various amounts of the coadsorbent CDCA, as specified in the Results and Discussion section. The staining time for all experiments was 20 h, and the electrodes were rinsed in acetonitrile and air dried in a dry box before assembly. Surlyn gaskets (35  $\mu\text{m}$ ) were melted between the working and counter electrodes (50 W heating element, 2 × 9 s for sufficient sealing).

The electrolyte contained 0.09 M [Cu(tmby)<sub>2</sub>](TFSI)<sub>2</sub>, 0.20 M [Cu(tmby)<sub>2</sub>](TFSI), 0.1 M LiTFSI, and 0.6 M 1-methylbenzimidazole in dry acetonitrile, and the DSSCs were filled with electrolyte by vacuum backfilling. The filling hole was sealed by Surlyn and a glass cover slip, before the protruding edges of the electrodes were covered with soldering tin for increased conductivity.

**Component and Device Characterization:** The UV–vis absorption measurements were recorded on a Hitachi U–1900 spectrophotometer, emission spectra were recorded with a F55 Spectrofluorometer from Edinburgh Instruments, and electrochemical experiments were recorded with a Versastat 3 potentiostat from Princeton Applied Research. Dye-loading experiments were conducted in duplicates by desorption of stained photoanodes in a solution of 40 mM tetrabutylammonium

hydroxide in stabilized THF. Separate molar extinction coefficients of the dyes in the basic media were measured for increased accuracy. The  $J$ - $V$  characteristics of the devices under 1 sun AM1.5 G illumination were recorded with an Oriol xenon lamp solar simulator (300 W), connected to a Keithley 2400, scanned from open circuit to short circuit with a settling time of 100 ms at each voltage step of 10 mV. IPCE measurements were recorded on a commercial Arkeo-Ariadne setup (Cicci Research s.r.l., 300 W xenon light source) with 50% sun bias light. For the  $J$ - $V$  sweeps and IPCE measurements, the devices were masked with a 0.158 cm<sup>2</sup> aperture black metal mask. Charge extraction and electron lifetime measurements were conducted using the Dyenamo Toolbox (Dyenamo, Sweden).

**Synthesis of (3S,7S,8S,9R,10R,13S,14R,17S)-17-((S)-5-((2-bromothiophen-3-yl)methoxy)pentan-2-yl)-10,13-dimethylhexadecahydro-1H-cyclopenta[a]phenanthrene-3,7-diol (9):** Compound **8** (3.01 g, 4.96 mmol), NaH (357 mg, 14.9 mmol), and THF (14 mL) were placed in a flask under nitrogen atmosphere and stirred for 1 h at 0 °C. 2-Bromo-3-bromomethylthiophene (1.90 g, 7.44 mmol) was added dropwise for 5 min before the reaction was heated to 60 °C and stirred for 19 h. The reaction mixture was cooled to room temperature and was quenched by addition of aqueous NH<sub>4</sub>Cl (5 wt%, 15 mL). The aqueous phase was extracted by ethyl acetate (3 × 50 mL), washed with brine (50 mL), and dried over anhydrous Na<sub>2</sub>SO<sub>4</sub> before the solvents were removed in vacuo. The crude product (light yellow oil) was then suspended in methanol (200 mL) and heated to 60 °C. HCl (37%, 10 mL) was added and the reaction stirred overnight. All solids dissolved during the reaction and TLC confirmed full conversion after 17 h. Aqueous NaHCO<sub>3</sub> solution (10 wt%, 150 mL) was added, and the aqueous phase was extracted by ethyl acetate (3 × 100 mL). The combined organic phases were washed with brine and dried over anhydrous Na<sub>2</sub>SO<sub>4</sub> before being concentrated in vacuo. The crude product was purified by silica gel column chromatography (ethyl acetate,  $R_f$  = 0.38) to yield compound **9** as a white solid (2.73 g, 4.93 mmol, 99%), mp 80–82 °C. <sup>1</sup>H NMR (600 MHz, acetone-*d*<sub>6</sub>) δ: 7.50 (d,  $J$  = 5.6 Hz, 1H), 7.04 (d,  $J$  = 5.6 Hz, 1H), 4.42 (s, 2H), 3.82–3.79 (m, 1H), 3.44 (t,  $J$  = 6.2 Hz, 2H), 3.36–3.30 (m, 1.4H\*), 3.16 (d,  $J$  = 3.2 Hz, 0.3H\*), 2.38–2.31 (m, 1H), 2.02–1.05 (m, 25H), 0.95 (d,  $J$  = 6.3 Hz, 3H), 0.92 (s, 3H), 0.69 (s, 3H); <sup>13</sup>C NMR (150 MHz, acetone-*d*<sub>6</sub>) δ: 140.3, 129.5, 127.4, 110.8, 72.1, 71.6, 68.1, 67.3, 57.2, 51.4, 43.3, 43.0, 40.86, 40.85, 40.6, 36.5, 36.02, 36.01, 33.8, 33.2, 31.7, 30.6, 29.2, 27.1, 24.4, 23.5, 21.6, 19.2, 12.3; IR (neat, cm<sup>-1</sup>) ν: 3394 (br), 2929 (m), 2863 (m), 1449 (w), 1374 (w), 1221 (w), 1108 (w), 1079 (w), 998 (w), 689 (w); HRMS (ESI+,  $m/z$ ): found 575.2177 (calcd. C<sub>29</sub>H<sub>45</sub><sup>79</sup>BrO<sub>3</sub>S 575.2170, [M + Na]<sup>+</sup>). The asterisk in (H\*) indicates exchange observed for the OH protons.

**Synthesis of 5-(3-(((4S)-4-((3S,7S,8S,9R,10R,13S,14R,17S)-3,7-dihydroxy-10,13-dimethylhexadecahydro-1H-cyclopenta[a]phenanthren-17-yl)pentyl)oxy)methyl)thiophen-2-yl)furan-2-carbaldehyde (10):** Compound **9** (500 mg, 0.903 mmol), (5-formylfuran-2-yl)boronic acid (379 mg, 2.71 mmol), PdCl<sub>2</sub>(dppf) (33 mg, 0.045 mmol), and K<sub>2</sub>CO<sub>3</sub> (499 mg, 3.61 mmol) were mixed. 1,4-Dioxane (6 mL) and water (6 mL) were degassed and added in a nitrogen atmosphere. The reaction mixture was heated to 80 °C and stirred for 25 min before being cooled to room temperature. Water (10 mL) was added and the aqueous phase extracted by ethyl acetate (3 × 50 mL). The combined organic phases were washed with brine (30 mL) and dried over anhydrous Na<sub>2</sub>SO<sub>4</sub>, filtered, and the solvents were removed in vacuo. The crude product was purified by silica gel column chromatography (ethyl acetate,  $R_f$  = 0.32) to obtain compound **10** as a light brown solid (350 mg, 0.615 mmol, 68%), mp 70–72 °C. <sup>1</sup>H NMR (600 MHz, acetone-*d*<sub>6</sub>) δ: 9.65 (s, 1H), 7.61 (d,  $J$  = 5.0 Hz, 1H), 7.54 (d,  $J$  = 3.7 Hz, 1H), 7.24 (d,  $J$  = 5.0 Hz, 1H), 6.92 (d,  $J$  = 3.7 Hz, 1H), 4.69 (s, 2H), 3.82–3.77 (m, 1H), 3.52 (t,  $J$  = 6.3 Hz, 2H), 3.37–3.30 (m, 1H), 3.38–3.31 (m, 1.5H\*), 3.16 (d,  $J$  = 3.2 Hz, 0.4H\*), 2.40–2.29 (m, 1H), 2.00–0.95 (m, 25H), 0.94 (d,  $J$  = 6.6 Hz, 3H), 0.91 (s, 3H), 0.67 (s, 3H); <sup>13</sup>C NMR (150 MHz, acetone-*d*<sub>6</sub>) δ: 177.6, 154.4, 152.8, 140.3, 131.4, 128.6, 127.6, 124.8, 110.7, 72.1, 71.6, 68.1, 67.2, 57.1, 51.2, 43.2, 42.9, 40.8, 40.7, 40.5, 36.4, 35.92, 35.90, 33.7, 33.2, 31.7, 30.3, 29.0, 27.1, 24.3, 23.4, 21.4, 19.1, 12.2; IR (neat, cm<sup>-1</sup>) ν: 3410 (br), 2930 (m), 2864 (m), 1673 (m), 1499 (w), 1377 (w), 1109 (w), 1079 (w), 1028 (w), 997 (w), 766 (w), 736 (w); HRMS (ESI+,  $m/z$ ): found

591.3120 (calcd. C<sub>34</sub>H<sub>48</sub>O<sub>5</sub>S 591.3120, [M + Na]<sup>+</sup>). The asterisk in (H\*) indicates exchange observed for the OH protons.

**Synthesis of 5-(5-bromo-3-(((4S)-4-((3S,7S,8S,9R,10R,13S,14R,17S)-3,7-dihydroxy-10,13-dimethylhexadecahydro-1H-cyclopenta[a]phenanthren-17-yl)pentyl)oxy)methyl)thiophen-2-yl)furan-2-carbaldehyde (11):** Compound **10** (230 mg, 0.404 mmol) was dissolved in a mixture of chloroform (3 mL) and glacial acetic acid (3 mL) in a nitrogen atmosphere at 0 °C. NBS (120 mg, 0.667 mmol) was added and the reaction was stirred in the dark, at 0 °C for 17 h, slowly reaching room temperature, before water (20 mL) was added and the aqueous phase was extracted by chloroform (3 × 30 mL). The combined organic phases were washed with brine (30 mL), dried over anhydrous Na<sub>2</sub>SO<sub>4</sub>, filtered, and concentrated in vacuo. Purification by silica gel column chromatography (ethyl acetate,  $R_f$  = 0.33) gave compound **11** as a brown solid (76 mg, 0.117 mmol, 29%), mp 83–85 °C. <sup>1</sup>H NMR (600 MHz, acetone-*d*<sub>6</sub>) δ: 9.66 (s, 1H), 7.54 (d,  $J$  = 3.8 Hz, 1H), 7.29 (s, 1H), 6.93 (d,  $J$  = 3.8 Hz, 1H), 4.66 (s, 2H), 3.82–3.77 (s, 1H), 3.52 (t,  $J$  = 6.3 Hz, 2H), 3.36–3.30 (m, 1H), 2.39–2.31 (m, 1H), 2.02–1.05 (m, 27H), 0.94 (d,  $J$  = 6.5 Hz, 3H), 0.92 (s, 3H), 0.68 (s, 3H); <sup>13</sup>C NMR (150 MHz, acetone-*d*<sub>6</sub>) δ: 177.8, 153.0, 152.7, 140.9, 134.2, 130.1, 124.6, 113.9, 111.3, 72.1, 71.7, 68.1, 66.9, 57.0, 51.3, 43.2, 42.9, 40.9, 40.8, 40.5, 36.44, 36.42, 35.95, 35.90, 33.7, 33.1, 31.7, 29.0, 27.0, 24.3, 23.4, 21.4, 19.1, 12.2; IR (neat, cm<sup>-1</sup>) ν: 3456 (br), 2932 (m), 2865 (m), 1710 (m), 1674 (m), 1497 (w), 1375 (w), 1243 (w), 1179 (w), 1078 (w), 978 (w), 766 (w), 735 (w); HRMS (ASAP+,  $m/z$ ): found 611.2189 (calcd. C<sub>34</sub>H<sub>44</sub>O<sub>3</sub>S<sup>79</sup>Br 611.2195, [M – 2H<sub>2</sub>O + H]<sup>+</sup>).

**Synthesis of 5-(5-(4-(bis(2',4'-dipropoxy-[1,1'-biphenyl]-4-yl)amino)phenyl)-3-(((4S)-4-((3S,7S,8S,9R,10R,13S,14R,17S)-3,7-dihydroxy-10,13-dimethylhexadecahydro-1H-cyclopenta[a]phenanthren-17-yl)pentyl)oxy)methyl)thiophen-2-yl)furan-2-carbaldehyde (14):** Compound **4** (72 mg, 0.10 mmol), PdCl<sub>2</sub>(CH<sub>3</sub>CN)<sub>2</sub> (0.53 mg, 2.04 μmol), and SPhos (3.4 mg, 8.2 μmol) were added to a Schlenk tube before it was evacuated, and a N<sub>2</sub> atmosphere established. Dry 1,4-dioxane (0.2 mL) was used to dissolve the compounds and the reaction mixture was stirred at room temperature before 4,4,5,5-tetramethyl-1,3,2-dioxaborolane (20 μL, 0.165 mmol) and dry triethylamine (130 μL) were added. The reaction mixture was heated to 80 °C and stirred for 1 h before cooling to room temperature. The reaction mixture was filtered through Celite using ethyl acetate as the eluent; the solvents were removed in vacuo. The crude mixture obtained was a yellow oil and was used without further purification.

The crude product from borylation, compound **11** (55 mg, 0.085 mmol), Pd(OAc)<sub>2</sub> (0.38 mg, 1.70 μmol), SPhos (1.4 mg, 3.4 μmol), and K<sub>2</sub>CO<sub>3</sub> (47 mg, 0.34 mmol) were mixed. 1,4-Dioxane (1 mL) and water (1 mL) were degassed and added in a nitrogen atmosphere. The reaction mixture was heated to 80 °C and stirred for 2 h before cooling to room temperature. Water (20 mL) was added and the aqueous phase extracted by ethyl acetate (3 × 25 mL). The combined organic phases were dried with brine (25 mL) and over anhydrous Na<sub>2</sub>SO<sub>4</sub>, filtered, and the solvents were removed in vacuo. The crude product was purified by silica gel column chromatography (n-pentane/ethyl acetate, 1:1,  $R_f$  = 0.16) to obtain compound **14** as a yellow solid (33 mg, 0.028 mmol, 33%), mp 108–110 °C. <sup>1</sup>H NMR (600 MHz, acetone-*d*<sub>6</sub>) δ: 9.65 (s, 1H), 7.65 (d,  $J$  = 8.8 Hz, 2H), 7.55–7.53 (m, 5H), 7.49 (s, 1H), 7.28 (d,  $J$  = 8.4 Hz, 2H), 7.18–7.15 (m, 4H), 7.13 (d,  $J$  = 8.7 Hz, 2H), 6.92 (d,  $J$  = 3.8 Hz, 1H), 6.64 (d,  $J$  = 2.3 Hz, 2H), 6.60 (dd,  $J$  = 8.5, 2.3 Hz, 2H), 4.69 (s, 2H), 3.99 (t,  $J$  = 6.5 Hz, 4H), 3.98 (t,  $J$  = 6.5 Hz, 4H), 3–80–3.75 (m, 1H), 3.56 (t,  $J$  = 6.1 Hz, 2H), 3.36–3.30 (m, 1.8H)\*, 3.09 (s, br., 0.7H)\*, 2.37–2.30 (m, 1H), 2.00–1.06 (m, 33H), 1.04 (t,  $J$  = 7.4 Hz, 6H), 1.00 (t,  $J$  = 7.4 Hz, 6H), 0.94 (d,  $J$  = 6.6 Hz, 3H), 0.90 (s, 3H), 0.66 (s, 3H); <sup>13</sup>C NMR (150 MHz, acetone-*d*<sub>6</sub>) δ: 177.4, 160.8 (2C), 158.0 (2C), 154.4, 152.6, 149.1, 146.2 (2C), 145.5, 141.5, 135.1 (2C), 131.6 (2C), 131.3 (4C), 127.6, 127.4 (2C), 126.4, 126.3, 125.1 (5C), 123.6 (2C), 123.4 (2C), 110.7, 106.8 (2C), 101.1 (2C), 72.1, 71.6, 70.6 (2C), 70.2 (2C), 68.1, 67.4, 57.1, 51.2, 43.2, 42.9, 40.8, 40.7, 40.5, 36.4, 35.91, 35.89, 33.6, 33.2, 31.7, 30.3, 29.0, 27.1, 24.3, 23.4, 23.33 (2C), 23.32 (2C), 21.4, 19.1, 12.2, 11.1 (2C), 10.8 (2C); IR (neat, cm<sup>-1</sup>) ν: 3413 (br), 2960 (m), 2928 (m), 2868 (m), 1672 (m), 1601 (m), 1490 (s), 1387 (s), 1271 (m), 1182 (s), 1133 (w), 1001 (w), 978 (m), 830 (m); HRMS (ESI+,  $m/z$ ): found 1196.6631 (calcd. C<sub>76</sub>H<sub>94</sub>NO<sub>9</sub>S 1196.6649, [M + H]<sup>+</sup>).

Synthesis of 5-(5-(4-(bis(2',4'-bis(hexyloxy)-[1,1'-biphenyl]-4-yl)amino)phenyl)-3-(((4S)-4-((3S,7S,8S,9R,10R,13S,14R,17S)-3,7-dihydroxy-10,13-dimethylhexadecahydro-1H-cyclopenta[a]phenanthren-17-yl)pentyl)oxy)methyl)thiophen-2-yl)furan-2-carbaldehyde (**15**): Compound **5** (133 mg, 0.151 mmol), PdCl<sub>2</sub>(CH<sub>3</sub>CN)<sub>2</sub> (0.8 mg, 3.0 μmol), and SPhos (5 mg, 12.0 μmol) were added to a Schlenk tube before it was evacuated, and an N<sub>2</sub> atmosphere was established. Dry 1,4-dioxane (0.3 mL) was used to dissolve the compounds and the reaction mixture was stirred at room temperature before 4,4,5,5-tetramethyl-1,3,2-dioxaborolane (33 μL, 0.227 mmol) and dry triethylamine (0.2 mL) were added. The reaction mixture was heated to 80 °C and stirred for 2.5 h before cooling to room temperature. The reaction mixture was filtered through Celite using ethyl acetate as the eluent. The solvents were removed in vacuo, giving the crude material as a yellow oil.

The crude product from borylation, compound **11** (70 mg, 0.108 mmol), Pd(OAc)<sub>2</sub> (0.5 mg, 2.161 μmol), SPhos (1.8 mg, 4.3 μmol), and K<sub>2</sub>CO<sub>3</sub> (60 mg, 0.43 mmol) were mixed. 1,4-Dioxane (1 mL) and water (1 mL) were degassed and added in a nitrogen atmosphere. The reaction mixture was heated to 80 °C and stirred for 35 min before cooling to room temperature. Water (20 mL) was added and the aqueous phase extracted by ethyl acetate (4 × 25 mL). The combined organic phases were dried with brine (30 mL) and over anhydrous Na<sub>2</sub>SO<sub>4</sub>, filtered, and the solvents were removed in vacuo. The crude product was purified by silica gel column chromatography (ethyl acetate, R<sub>f</sub> = 0.48) to obtain compound **15** as a yellow solid (46 mg, 0.034 mmol, 31%), mp 78–79 °C. <sup>1</sup>H NMR (600 MHz, acetone-d<sub>6</sub>) δ: 9.65 (s, 1H), 7.65 (d, J = 8.7 Hz, 2H), 7.56–7.52 (m, 5H), 7.49 (s, 1H), 7.28 (d, J = 8.5 Hz, 2H), 7.19–7.15 (m, 4H), 7.14 (d, J = 8.7 Hz, 2H), 6.92 (d, J = 4.0 Hz, 1H), 6.65 (d, J = 2.4 Hz, 2H), 6.60 (dd, J = 8.5, 2.4 Hz, 2H), 4.70 (s, 2H), 4.05–4.02 (m, 8H), 3.79–3.75 (m, 1H), 3.56 (t, J = 6.1 Hz, 2H), 3.35–3.30 (m, 1H), 2.33 (q, J = 12.2 Hz, 1H), 2.00–1.01 (m, 60H), 0.94 (d, J = 6.6 Hz, 3H), 0.92 (t, J = 7.0 Hz, 6H), 0.90 (s, 3H), 0.87 (t, J = 7.0 Hz, 6H), 0.66 (s, 3H); <sup>13</sup>C NMR (150 MHz, acetone-d<sub>6</sub>) δ: 177.4, 160.8 (2C), 158.0 (2C), 154.3, 152.7, 149.2, 146.2 (2C), 145.5, 141.5, 135.1 (2C), 131.6 (2C), 131.3 (4C), 127.6, 127.4 (2C), 126.34, 126.29, 125.0 (5C), 123.6 (2C), 123.4 (2C), 110.7, 106.8 (2C), 101.1 (2C), 72.0, 71.6, 69.0 (2C), 68.6 (2C), 68.0, 67.5, 57.1, 51.2, 43.2, 42.9, 40.8, 40.7, 40.5, 36.43, 36.36, 35.9, 33.7, 33.2, 32.4 (2C), 32.3 (2C), 31.7, 30.3, 30.0 (2C), 29.9 (2C), 29.0, 27.1, 26.6 (2C), 26.5 (2C), 24.3, 23.4, 23.3 (4C), 21.4, 19.1, 14.4 (2C), 14.3 (2C), 12.2; IR (neat, cm<sup>-1</sup>) ν: 3458 (br), 2931 (m), 2862 (m), 1675 (m), 1603 (m), 1492 (m), 1288 (m), 1182 (m), 830 (m); HRMS (ESI+, m/z): found 1364.8512 (calcd. C<sub>88</sub>H<sub>118</sub>NO<sub>9</sub>S 1364.8527, [M + H]<sup>+</sup>).

Synthesis of (E)-3-(5-(5-(4-(bis(2',4'-dipropoxy-[1,1'-biphenyl]-4-yl)amino)phenyl)-3-(((4S)-4-((3S,7S,8S,9R,10R,13S,14R,17S)-3,7-dihydroxy-10,13-dimethylhexadecahydro-1H-cyclopenta[a]phenanthren-17-yl)pentyl)oxy)methyl)thiophen-2-yl)furan-2-yl)-2-cyanoacrylic acid (Dye C<sub>3</sub>-CDCA): Compound **14** (32 mg, 0.027 mmol) and cyanoacetic acid (46 mg, 0.54 mmol) were dissolved in degassed acetonitrile (12 mL) and THF (2 mL) in a nitrogen atmosphere. Piperidine (32 μL, 27 mg, 0.321 mmol) was added and the reaction was heated to 80 °C for 2 h before cooling to room temperature and quenched in HCl (1 M, 50 mL). Ethyl acetate (30 mL) was added and the organic phase was washed with water (3 × 200 mL), then dried with brine (30 mL) and over anhydrous Na<sub>2</sub>SO<sub>4</sub>, filtered, and the solvents were removed in vacuo. The crude product was purified by silica gel column chromatography (gradient: 0–20% MeOH in ethyl acetate). The solvents were removed, the product redissolved in ethyl acetate, and then filtered before complete removal of the solvents yielded sensitizer C<sub>3</sub>-CDCA as a dark solid (18 mg, 0.014 mmol, 54%), mp 153–154 °C (dec. 173 °C). <sup>1</sup>H NMR (600 MHz, THF-d<sub>8</sub>) δ: 7.86 (s, 1H), 7.46 (d, J = 8.3 Hz, 2H), 7.38–7.35 (m, 5H), 7.32 (s, 1H), 7.13 (d, J = 8.4 Hz, 2H), 7.04–7.01 (m, 6H), 6.80 (br. s, 1H), 6.48 (d, J = 2.3 Hz, 2H), 6.43 (dd, J = 8.4, 2.2 Hz, 2H), 4.65 (s, 2H), 3.85–3.80 (m, 8H), 3.59 (s, 1H), 3.50–3.40 (m, 3H), 3.35 (s, br, 0.4H\*), 3.14–3.08 (m, 1H), 2.23–2.15 (m, 1H), 1.89–0.97 (m, 33H), 0.94 (t, J = 7.4 Hz, 6H), 0.89 (t, J = 7.5 Hz, 6H), 0.84 (d, J = 6.6 Hz, 3H), 0.78 (s, 3H), 0.56 (s, 3H) (CO<sub>2</sub>H proton missing); <sup>13</sup>C NMR (150 MHz, acetone-d<sub>6</sub>) δ: 163.0, 159.5 (2C), 156.6 (2C), 154.0, 147.9, 147.7, 145.0 (2C), 144.8, 140.7, 136.4, 133.7 (2C), 130.1 (2C), 129.8, 129.7 (4C), 126.6, 125.9 (2C), 124.6, 123.6, 123.5 (5C), 122.5 (2C), 122.3

(2C), 115.0, 110.3, 105.0 (2C), 99.8 (2C), 70.7, 70.4, 69.3 (2C), 68.7 (2C), 66.8, 66.7, 55.9, 50.0, 41.9, 41.8, 39.6, 39.5, 39.4, 35.35, 35.32, 34.9, 34.7, 32.3, 32.0, 30.6, 27.9, 26.0, 23.1, 22.2 (2C), 22.13 (2C), 22.05, 20.2, 17.8, 10.9, 9.8 (2C), 9.5 (2C); IR (neat, cm<sup>-1</sup>) ν: 3400 (br), 2961 (m), 2931 (m), 2870 (m), 2217 (w), 1704 (w), 1601 (m), 1488 (s), 1387 (m), 1264 (m), 1181 (s), 1030 (m), 829 (m), 734 (s); HRMS (APPI-, m/z): found 1261.6573 (calcd. C<sub>79</sub>H<sub>93</sub>N<sub>2</sub>O<sub>10</sub>S 1261.6551, [M - H]<sup>-</sup>). The asterisk in (H\*) indicates exchange observed for the OH protons.

Synthesis of (E)-3-(5-(5-(4-(bis(2',4'-bis(hexyloxy)-[1,1'-biphenyl]-4-yl)amino)phenyl)-3-(((4S)-4-((3S,7S,8S,9R,10R,13S,14R,17S)-3,7-dihydroxy-10,13-dimethylhexadecahydro-1H-cyclopenta[a]phenanthren-17-yl)pentyl)oxy)methyl)thiophen-2-yl)furan-2-yl)-2-cyanoacrylic acid (Dye C<sub>6</sub>-CDCA): Compound **15** (45 mg, 0.033 mmol) and cyanoacetic acid (56 mg, 0.66 mmol) were dissolved in degassed acetonitrile (35 mL) and THF (5 mL) in a nitrogen atmosphere. Piperidine (39 μL, 34 mg, 0.396 mmol) was added and the reaction was heated to 80 °C for 1 h before cooling to room temperature and quenched in HCl (1 M, 100 mL). Ethyl acetate (30 mL) was added and the organic phase was washed with water (3 × 200 mL), then dried with brine (30 mL) and over anhydrous Na<sub>2</sub>SO<sub>4</sub>, filtered, and the solvents were removed in vacuo. The crude product was purified by silica gel column chromatography (gradient: 0–30% MeOH in ethyl acetate). The solvents were removed, the product redissolved in ethyl acetate, and then filtered before complete removal of the solvents yielded the sensitizer C<sub>6</sub>-CDCA as a dark solid (45 mg, 0.031 mmol, 95%), mp 132–134 °C (dec. 163 °C). <sup>1</sup>H NMR (600 MHz, THF-d<sub>8</sub>) δ: 7.85 (s, 1H), 7.45 (d, J = 8.50 Hz, 2H), 7.39–7.33 (m, 5H), 7.31 (s, 1H), 7.12 (d, J = 8.4 Hz, 2H), 7.05–7.00 (m, 6H), 6.78 (br. s, 1H), 6.47 (d, J = 2.1 Hz, 2H), 6.43 (dd, J = 8.5, 2.1 Hz, 2H), 4.64 (s, 2H), 3.89–3.84 (m, 8H), 3.61–3.58 (m, 1H), 3.44–3.40 (m, 2H), 3.15–3.09 (m, 2H), 2.23–2.15 (m, 1H), 1.90–0.84 (m, 58H), 0.84–0.71 (m, 18H), 0.56 (s, 3H) (CO<sub>2</sub>H proton missing); <sup>13</sup>C NMR (150 MHz, THF-d<sub>8</sub>) δ: 163.2, 159.5 (2C), 156.6 (2C), 153.6, 147.8 (2C), 144.9 (2C), 144.7, 140.5, 136.1, 133.7 (2C), 130.0 (2C), 129.8, 129.7 (4C), 126.6, 125.9 (2C), 124.6, 123.8, 123.5 (5C), 122.5 (2C), 122.3 (2C), 115.2, 110.2, 104.9 (2C), 99.8 (2C), 70.7, 70.4, 67.7 (2C), 67.2 (2C), 66.8, 66.7, 55.9, 50.0, 41.9, 41.8, 39.6, 39.5, 39.4, 35.33, 35.31, 34.9, 34.6, 32.3, 32.0, 31.2 (2C), 31.1 (2C), 30.6, 28.9 (2C), 28.7 (2C), 27.8, 26.0, 25.4 (4C), 23.1, 22.2 (2C), 22.14 (2C), 22.05, 20.2, 17.8, 13.1 (2C), 13.0 (2C), 10.9; IR (neat, cm<sup>-1</sup>) ν: 3387 (br), 2927 (m), 2858 (m), 2217 (w), 1700 (w), 1601 (m), 1489 (s), 1380 (m), 1263 (s), 1180 (s), 1030 (m), 794 (m), 735 (m); HRMS (ESI, m/z): found 1429.8400 (calcd. C<sub>91</sub>H<sub>117</sub>N<sub>2</sub>O<sub>10</sub>S 1429.8429, [M - H]<sup>-</sup>).

## Supporting Information

Supporting Information is available from the Wiley Online Library or from the author.

## Acknowledgements

The authors thank MSc Ingunn Schröder for embarking on the chemistry of CDCA as a preliminary investigation for this work. The authors acknowledge staff engineer Roger Aarvik and Ph.D. Susana Villa Gonzalez for their technical and mass spectrometry contributions. The support from the Research Council of Norway to the Norwegian NMR Platform (project number 226244/F50) is much appreciated.

## Conflict of Interest

The authors declare no conflict of interest.

## Keywords

antiaggregation, chenodeoxycholic acid, dye design, dye distributions, sensitizer quantum efficiencies



Received: December 20, 2019

Revised: January 27, 2020

Published online:

- [1] B. O'Regan, M. Grätzel, *Nature* **1991**, 353, 737.
- [2] A. Hagfeldt, G. Boschloo, L. Sun, L. Kloo, H. Pettersson, *Chem. Rev.* **2010**, 110, 6595.
- [3] M. Freitag, J. Teuscher, Y. Saygili, X. Zhang, F. Giordano, P. Liska, J. Hua, S. M. Zakeeruddin, J.-E. Moser, M. Grätzel, A. Hagfeldt, *Nat. Photonics* **2017**, 11, 372.
- [4] D. Joly, L. Pelleja, S. Narbey, F. Oswald, T. Meyer, Y. Kervella, P. Maldivi, J. N. Clifford, E. Palomares, R. Demadrille, *Energy Environ. Sci.* **2015**, 8, 2010.
- [5] N. Robertson, *Angew. Chem. Int. Ed.* **2006**, 45, 2338.
- [6] Y. S. Tingare, N. S. Vinh, H.-H. Chou, Y.-C. Liu, Y.-S. Long, T.-C. Wu, T.-C. Wei, C.-Y. Yeh, *Adv. Energy Mater.* **2017**, 7, 1700032.
- [7] E. Mosconi, J.-H. Yum, F. Kessler, C. J. Gómez García, C. Zuccaccia, A. Cinti, M. K. Nazeeruddin, M. Grätzel, F. De Angelis, *J. Am. Chem. Soc.* **2012**, 134, 19438.
- [8] S. M. Feldt, E. A. Gibson, E. Gabrielsson, L. Sun, G. Boschloo, A. Hagfeldt, *J. Am. Chem. Soc.* **2010**, 132, 16714.
- [9] L. Zhang, J. M. Cole, *J. Mater. Chem. A* **2017**, 5, 19541.
- [10] X. Zhang, Y. Xu, F. Giordano, M. Schreier, N. Pellet, Y. Hu, C. Yi, N. Robertson, J. Hua, S. M. Zakeeruddin, H. Tian, M. Grätzel, *J. Am. Chem. Soc.* **2016**, 138, 10742.
- [11] K. Kakiage, Y. Aoyama, T. Yano, K. Oya, J.-i. Fujisawa, M. Hanaya, *Chem. Commun.* **2015**, 51, 15894.
- [12] A. Yella, R. Humphry-Baker, B. F. E. Curchod, N. Ashari-Astani, J. Teuscher, L. E. Polander, S. Mathew, J.-E. Moser, I. Tavernelli, U. Rothlisberger, M. Grätzel, M. K. Nazeeruddin, J. Frey, *Chem. Mater.* **2013**, 25, 2733.
- [13] M. Xu, R. Li, N. Pootrakulchote, D. Shi, J. Guo, Z. Yi, S. M. Zakeeruddin, M. Grätzel, P. Wang, *J. Phys. Chem. C* **2008**, 112, 19770.
- [14] J.-H. Yum, D. P. Hagberg, S.-J. Moon, K. M. Karlsson, T. Marinado, L. Sun, A. Hagfeldt, M. K. Nazeeruddin, M. Grätzel, *Angew. Chem. Int. Ed.* **2009**, 48, 1576.
- [15] S. Mathew, A. Yella, P. Gao, R. Humphry-Baker, B. F. E. Curchod, N. Ashari-Astani, I. Tavernelli, U. Rothlisberger, K. Nazeeruddin, M. Grätzel, *Nat. Chem.* **2014**, 6, 242.
- [16] N. Manfredi, M. Monai, T. Montini, F. Peri, F. De Angelis, P. Fornasiero, A. Abbotto, *ACS Energy Lett.* **2018**, 3, 85.
- [17] A. Kay, M. Grätzel, *J. Phys. Chem.* **1993**, 97, 6272.
- [18] J. M. Donkers, R. L. P. Roscam Abbing, S. F. J. van de Graaf, *Biochem. Pharmacol.* **2019**, 161, 1.
- [19] N. A. Malik, *Appl. Biochem. Biotechnol.* **2016**, 179, 179.
- [20] R. Cisneros, M. Beley, F. Lapique, *Phys. Chem. Chem. Phys.* **2016**, 18, 9645.
- [21] A. F. Buene, E. E. Ose, A. G. Zakariassen, A. Hagfeldt, B. H. Hoff, *J. Mater. Chem. A* **2019**, 7, 7581.
- [22] Y. Hong, Z. Iqbal, X. Yin, D. Cao, *Tetrahedron* **2014**, 70, 6296.
- [23] H. Cheema, A. Baumann, E. K. Loya, P. Brogdon, L. E. McNamara, C. A. Carpenter, N. I. Hammer, S. Mathew, C. Risko, J. H. Delcamp, *ACS Appl. Mater. Interfaces* **2019**, 11, 16474.
- [24] Y. Saygili, M. Söderberg, N. Pellet, F. Giordano, Y. Cao, A. B. Muñoz-García, S. M. Zakeeruddin, N. Vlachopoulos, M. Pavone, G. Boschloo, L. Kavan, J.-E. Moser, M. Grätzel, A. Hagfeldt, M. Freitag, *J. Am. Chem. Soc.* **2016**, 138, 15087.
- [25] Y. Saygili, M. Stojanovic, N. Flores-Díaz, S. M. Zakeeruddin, N. Vlachopoulos, M. Grätzel, A. Hagfeldt, *Inorganics* **2019**, 7, 30.
- [26] J. T. Lin, P.-C. Chen, Y.-S. Yen, Y.-C. Hsu, H.-H. Chou, M.-C. P. Yeh, *Org. Lett.* **2009**, 11, 97.
- [27] J. Zhao, T. Jin, A. Islam, E. Kwon, M. Akhtaruzzaman, N. Asao, L. Han, K. A. Alamry, S. A. Kosa, A. M. Asiri, Y. Yamamoto, *Tetrahedron* **2014**, 70, 6211.
- [28] H. Zhu, Y. Wu, J. Liu, W. Zhang, W. Wu, W.-H. Zhu, *J. Mater. Chem. A* **2015**, 3, 10603.
- [29] K.-M. Lu, W.-M. Li, P.-Y. Lin, K.-T. Liu, C.-Y. Liu, *Adv. Synth. Catal.* **2017**, 359, 3805.
- [30] A. Baumann, H. Cheema, M. A. Sabuj, L. E. McNamara, Y. Zhang, A. Peddapuram, S. T. Nguyen, D. L. Watkins, N. I. Hammer, N. Rai, J. H. Delcamp, *Phys. Chem. Chem. Phys.* **2018**, 20, 17859.
- [31] Y. Cao, Y. Liu, S. M. Zakeeruddin, A. Hagfeldt, M. Grätzel, *Joule* **2018**, 2, 1108.
- [32] Y. Hao, Y. Saygili, J. Cong, A. Eriksson, W. Yang, J. Zhang, E. Polanski, K. Nonomura, S. M. Zakeeruddin, M. Grätzel, A. Hagfeldt, G. Boschloo, *ACS Appl. Mater. Interfaces* **2016**, 8, 32797.
- [33] M. Freitag, F. Giordano, W. Yang, M. Pazoki, Y. Hao, B. Zietz, M. Grätzel, A. Hagfeldt, G. Boschloo, *J. Phys. Chem. C* **2016**, 120, 9595.
- [34] J.-H. Yum, E. Baranoff, F. Kessler, T. Moehl, S. Ahmad, T. Bessho, A. Marchioro, E. Ghadiri, J.-E. Moser, C. Yi, M. K. Nazeeruddin, M. Grätzel, *Nat. Commun.* **2012**, 3, 631.
- [35] M. Freitag, Q. Daniel, M. Pazoki, K. Sveinbjörnsson, J. Zhang, L. Sun, A. Hagfeldt, G. Boschloo, *Energy Environ. Sci.* **2015**, 8, 2634.
- [36] E. Gabrielsson, H. Ellis, S. Feldt, H. Tian, G. Boschloo, A. Hagfeldt, L. Sun, *Adv. Energy Mater.* **2013**, 3, 1647.
- [37] K. L. Billingsley, S. L. Buchwald, *J. Org. Chem.* **2008**, 73, 5589.
- [38] T. Bjørnholm, D. R. Greve, N. Reitzel, T. Hassenkam, K. Kjaer, P. B. Howes, N. B. Larsen, J. Bøgelund, M. Jayaraman, P. C. Ewbank, R. D. McCullough, *J. Am. Chem. Soc.* **1998**, 120, 7643.
- [39] Q.-Y. Yu, J.-Y. Liao, S.-M. Zhou, Y. Shen, J.-M. Liu, D.-B. Kuang, C.-Y. Su, *J. Phys. Chem. C* **2011**, 115, 22002.
- [40] Y. Hua, S. Chang, D. D. Huang, X. Zhou, X. J. Zhu, J. Z. Zhao, T. Chen, W. Y. Wong, W. K. Wong, *Chem. Mater.* **2013**, 25, 2146.
- [41] L. Schmidt-Mende, J. E. Kroeze, J. R. Durrant, M. K. Nazeeruddin, M. Grätzel, *Nano Lett.* **2005**, 5, 1315.
- [42] V. V. Pavlishchuk, A. W. Addison, *Inorganica Chim. Acta* **2000**, 298, 97.
- [43] D. P. Hagberg, X. Jiang, E. Gabrielsson, M. Linder, T. Marinado, T. Brinck, A. Hagfeldt, L. Sun, *J. Mater. Chem.* **2009**, 19, 7232.
- [44] Y. Saygili, M. Stojanovic, H. Michaels, J. Tjepelt, J. Teuscher, A. Massaro, M. Pavone, F. Giordano, S. M. Zakeeruddin, G. Boschloo, J.-E. Moser, M. Grätzel, A. B. Muñoz-García, A. Hagfeldt, M. Freitag, *ACS Appl. Energy Mater.* **2018**, 1, 4950.
- [45] J.-H. Yum, T. W. Holcombe, Y. Kim, J. Yoon, K. Rakstys, M. K. Nazeeruddin, M. Grätzel, *Chem. Commun.* **2012**, 48, 10727.
- [46] Md. K. Nazeeruddin, M. Grätzel, E. Baranoff, F. Kessler, J.-H. Yum, EP2492277A1, École Polytechnique Fédérale de Lausanne **2011**.
- [47] L. Huang, Y. Sun, H. Zhu, Y. Zhang, J. Xu, Y.-M. Shen, *Steroids* **2009**, 74, 701.
- [48] C. D'Amore, F. S. Di Leva, V. Sepe, B. Renga, C. Del Gaudio, M. V. D'Auria, A. Zampella, S. Fiorucci, V. Limongelli, *J. Med. Chem.* **2014**, 57, 937.
- [49] P. R. Parry, M. R. Bryce, B. Tarbit, *Org. Biomol. Chem.* **2003**, 1, 1447.
- [50] S.-H. Kim, R. D. Rieke, *J. Org. Chem.* **2013**, 78, 1984.
- [51] H. Ellis, R. Jiang, S. Ye, A. Hagfeldt, G. Boschloo, *Phys. Chem. Chem. Phys.* **2016**, 18, 8419.